Stochastic evolution of a turbulent interface in a shear flow

Yohann Duguet[1] & Philipp Schlatter[2]

[1] LIMSI-CNRS, UPR 3251, Université Paris-Sud, 91403 Orsay CEDEX, France
[2] Linné Flow Centre, KTH Mechanics, Osquars Backe 18, Stockholm, SE-10044, Suède/Sweden
duguet@limsi.fr

Résumé. L'écoulement de Couette plan, confiné entre deux plaques parallèles qui cisaillent le fluide, est un exemple classique où la transition vers la turbulence se produit de manière sous-critique, c'est-à-dire malgré la stabilité linéaire de l'écoulement de base. Ici nous nous intéressons à la compétition spatio-temporelle entre la phase turbulente (active) et la phase laminaire (absorbante). En particulier, des simulations numériques montrent que l'interface délimitant ces deux phases, lorsqu'elle est parallèle à l'écoulement moyen, se déplace d'une manière stochastique qui peut être modélisée comme une marche aléatoire continue en temps. L'analyse statistique suggère un processus de diffusion gaussien et permet de déterminer la vitesse moyenne de cette interface en fonction du nombre de Reynolds, ainsi que la valeur seuil au-delà de laquelle la turbulence contamine tout le domaine. Pour les nombres de Reynolds les plus bas, cette dynamique stochastique entre en compétition avec une dynamique de croissance déterministe des perturbations localisées. Cette dernière dynamique inattendue résulte de l'existence d'un régime, dit de *snaking*, où cohabitent de multiples solutions localisées et instables des équations de Navier-Stokes.

Abstract. Plane Couette flow, the flow sheared between two parallel counter-sliding plates, is a classical example where transition to turbulence proceeds in a subcritical way, i.e. despite the linear stability of the base state. We are here interested in the spatio-temporal competition between the (active) turbulent phase and the (absorbing) laminar one. In particular, numerical simulations show that the interface delimiting those two phases, when parallel to the mean flow, moves in a stochastic manner which can be modelled as a continuous-time random walk. Statistical analysis suggests a Gaussian diffusion process and allows one to derive the mean drift velocity of this interface as a function of the Reynolds number, as well as the threshold value above which turbulence contaminates the whole domain. For the lowest values of the Reynolds number, the stochastic dynamics competes with a determistic growth regime of localised perturbations. The latter, rather unexpectedly, is related to the existence of a *snaking* regime where multiple unstable localised solutions of the Navier-Stokes equations co-exist.

1 Statistical analysis

In this study we are interested in determining numerically the velocity at which a laminar/turbulent interfaces moves through a shear flow. Because of its simplicity, we will consider the example of plane Couette flow, which has zero net flux. Plane Couette flow is the flow sheared between two parallel plates of velocities $\pm U$ in the streamwise direction x, separated by a gap $2h$ in the wall-normal direction y. The spanwise direction is noted z. The three-dimensional flow is governed by the incompressible Navier-Stokes equations with no-slip boundary conditions at both walls $y = \pm 1$. Velocities, time and space are non-dimensionalised by U, h and $\frac{h}{U}$, respectively. It is known that this flow admits a steady 1D solution $u(y) = \frac{Uy}{h}$ which is linearly stable for all Re, where $Re = \frac{Uh}{\nu}$ is the Reynolds number, with ν the kinematic viscosity of the fluid.

The spectral representation of the flow is based on Chebyshev polynomials in the y-direction, and a discrete Fourier decomposition in both x and z. This implies periodic boundary conditions in the in-plane directions, with the associated wavelengths noted respectively L_x and L_z. Time-stepping is achieved by a fourth-order Runge-Kutta integrator with adaptative variable timestep. The number of spectral modes is determined by the triplet $\boldsymbol{N} = (N_x, N_y, N_z)$, with the extra use of a $\frac{3}{2}$-dealiasing rule for the evaluation of the nonlinear terms. We perform well-resolved simulations in a domain $D1$ of size $(L_x, L_z) = (10.417, 250)$, using a resolution $\boldsymbol{N} = (32, 49, 1024)$. For the simulations at the lowest values of Re, the slow spreading

of localised perturbations made it possible to use a shorter domain $D2$ of size $(L_x, L_z) = (10.417, 125)$ with half the number of collocations points in the spanwise direction, i.e. $\boldsymbol{N} = (32, 49, 512)$. The short streamwise extent L_x is used as a numerical trick forcing potential laminar/turbulent interfaces to be orthogonal to the spanwise direction z, preventing the formation of a secondary large-scale flow around localised spots. Note that a very similar geometry has been used by Barkley & Tuckerman (Fig. 15 in [7]) in quenching experiments with $(L_x, L_z) = (10, 120)$. More recently, edge states and other finite-amplitude solutions were found in a similar geometry with $(4\pi, 16\pi)$[6].

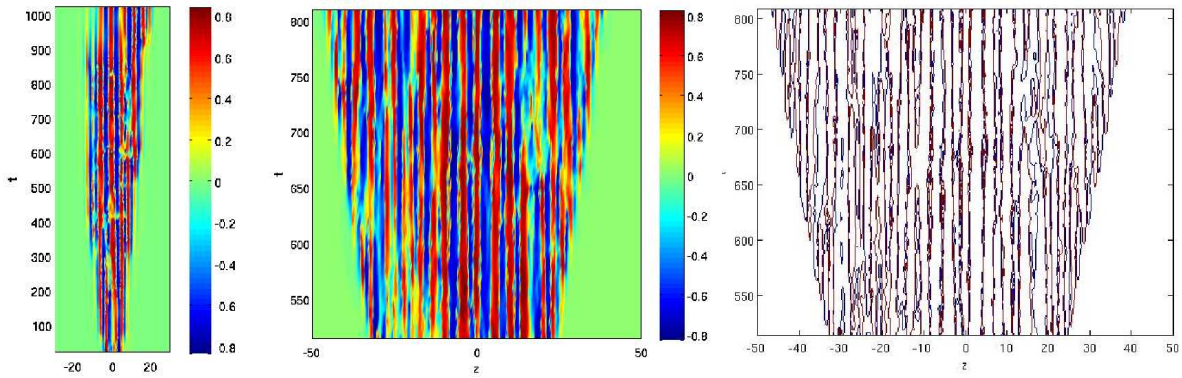

FIG. **1.** Space-time (z, t) diagrams for $Re = 350$ (left) and Re=500 (middle,right). Displayed are the quantity $Y(z, t)$ (left, middle) and the iso-contours $Y(z, t) = \pm 0.2$ (right)

The diagrams shown in Figure 1 and 5 corresponds to two realisations at $Re = 350$ and $Re = 500$. The visualised quantity corresponds here to

$$Y(z, t) = \{y | \langle u \rangle_x = 0\}, \tag{1}$$

the wall-normal coordinate of the $< u >_x = 0$ iso-surface, where $< u >_x$ is the streamwise velocity averaged over the wavelength L_x. This quantity has been chosen because it is zero in the laminar phase and departs away from zero in the presence of turbulent bursts. Taking $|Y| = 0.2$ in Eq. 1as a criterion to locate the laminar/turbulent interface in absolute value has proven a robust choice.

The turbulent zone is here delimited by two asymmetric fronts. Each of the two fronts clearly moves from or towards the turbulent area in discrete steps, gaining or losing one streak (occasionnally several streaks). The time interval between two successive events is not constant, requesting statistical description. The distance along which the front has progressed or retreated during one of these events is also not constant, firstly because streaks do not possess a uniquely defined spanwise wavelength, secondly because several streaks can be gained or lost at the same time. A convenient description of the motion of each front, well-adapted to a statistical analysis, is possible within the frame of continuous-time random walks (CTRW) [5]. Retreat and progress of a given interface are seen here as two competing and complementary events occuring suddenly on a distance Δz (the "jump length") after a time T ("the waiting time"). The CTRW process is here as asymmetric since the probabilities for the two events is not expected to be identical, statistically inducing a drift of the front in one direction or the other. If g refers to progress events and r to retreat events, four cumulative probability distributions are needed to characterise the whole process :

- $P_g(T > t)$ (resp. $P_r(T > t)$) : the probability that the next event be a *progress* (resp. *retreat*) event after a waiting time T being larger than a time t ;
- $P_g(\Delta z > L)$ (resp. $P_r(\Delta z > L)$) : the probability that the next event be a *progress* (resp. *retreat*) event with a jump length Δz being larger than a distance L.

Proper application of this formalism demands that Δz and T be treated as statistically independent variables, and that Δz and T be independent of time and space, i.e. that the statistical properties of

those two variables do not depend of the current position of the front. By convention we will consider all values of Δz positive, assuming that a positive drift corresponds to a g event and a negative drift to a r event. The various values of Δz and T are directly measured from diagrams such as Fig. 1 (right). They are gathered over a large number of independent realisations for each value of Re in the range $[230 : 650]$, yielding the four cumulative probability distributions required. Fig. 2 clearly suggests that the cumulative distributions P_g and P_r for the waiting times are well fitted by exponential distributions. This corresponds to a memoryless process for the waiting times regardless of which event is considered ("g" or "r"). Exponential scaling also holds reasonably well for the cumulative distributions of the jump lengths, see Fig. 3. The implications are strong : as long as the exponential scaling holds, the motion of the front can be thought of as a Gaussian (normal) diffusion process.

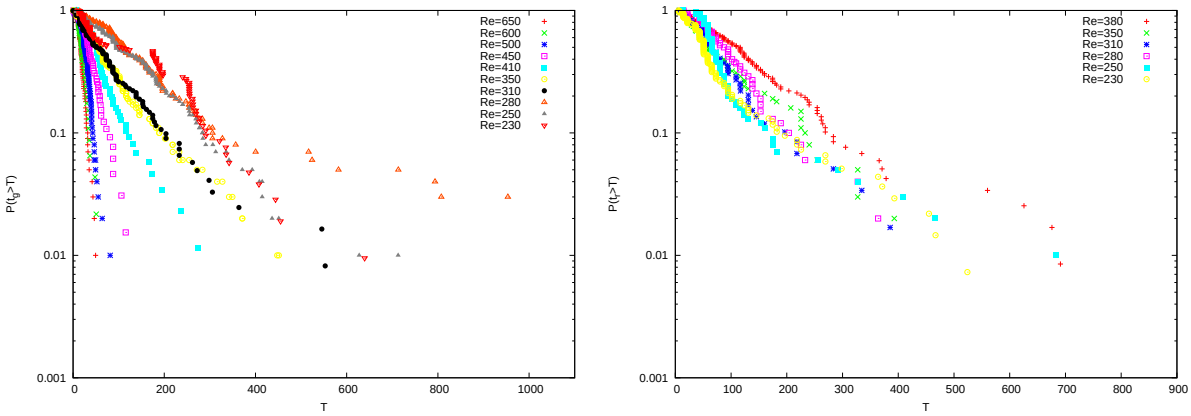

FIG. **2.** Cumulative probability distributions for the waiting times $P_g(T > t)$ (top) and $P_r(T > t)$ (bottom) for various values of Re.

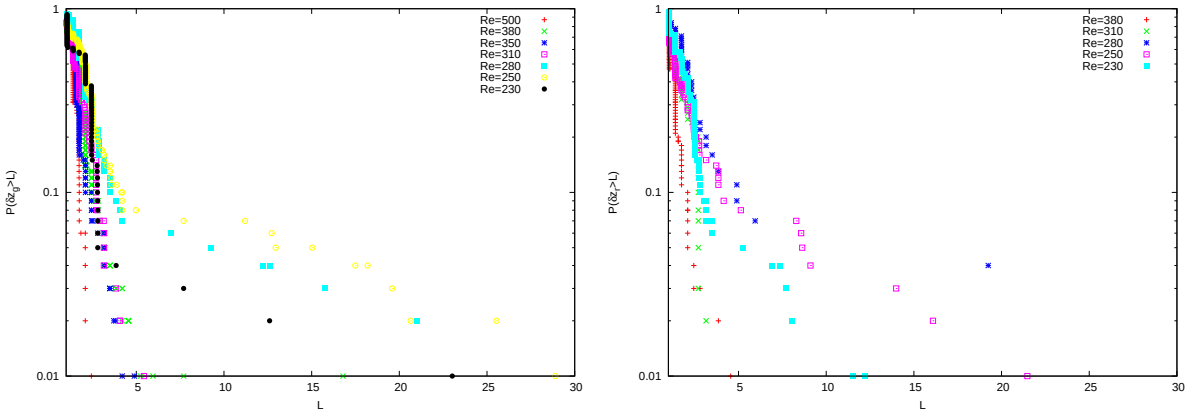

FIG. **3.** Cumulative probability distributions for the waiting times $P_g(\Delta z > L)$ (top) and $P_g(\Delta z > L)$ (bottom) for various values of Re.

A comparison of the distributions corresponding to nearly all values of Re investigated is shown in Figure 2 for the waiting times and Figure 3 for the jump lengths. A clear Poissonian trend emerges for $P_g(T)$ and $P_g(\Delta z)$ for $Re \geq 300$ with a slope monotonously decreasing with Re. The cases $250 \leq Re \leq 290$ are less clearly amenable to an interpretation as a memory-less process, because of the presence of extreme events (very long waiting times and/or long jumps). The data is here insufficient to decide whether

the extreme events only produce unconverged statistics (still ruled by Poissonian dynamics) or if another tail is emerging with a different (possibly anomalous) scaling. For $Re = 230$ (see Fig. 2) and below (not shown), the global deviation from exponential is strong, suggesting a different process. Description of the retreat statistics $P_r(T)$ and $P_r(\Delta z)$ reveals the same trends, however there slopes increase in absolute value with increasing Re. Furthermore, the analysis is blurred at high Re by the rarity of retreat events compared to progress events : above $Re \geq 400$, the occurence of retreat events would demand too much simulation time (or equivalently too many independent realisations) to produce converged statistics.

Interpolation of the slopes in Fig. 2 directly yields the average values. We exploit this property to compute the conditional averages $\langle T_g \rangle$ (resp. $\langle T_r \rangle$), i.e. the average waiting time given that the next event is a "g" event (resp. an "r" event), and equivalently the conditional averages $\langle \Delta z_g \rangle$ and $\langle \Delta z_r \rangle$. Error bars are computed by comparing undersampled distributions in a Bayesian way, constantly excluding events depicted as rare ones. As expected from Fig. 2, Fig. 4 (left) shows that the conditional average time $\langle T_g \rangle$ decreases monotonously with Re while $\langle T_r \rangle$ monotonously increases with it. The two averages thus safely cross at a given value of Re, $Re_{c1} = 320 \pm 10$. The interpretation is straightforward : for $Re > Re_{c1}$, the probability is higher than the next event shall be a progress event than a retreat event, regardless of the history of the front, while retreat events are favoured statistically for $Re < Re_{c1}$. The two average times coincide exactly only for $Re = Re_{c1}$. Note the closeness of Re_{c1} to the experimental thresholds $Re_g \approx 325$ in large domains. Strictly speaking, this does not mean that the front is statistically steady at $Re = Re_{c1}$ since the jump length distributions must also be included in the picture. Figure 4 (right) shows that $\langle \Delta z_g \rangle$ decreases slowly with Re. $\langle \Delta z_r \rangle$, in the range where data is available, also shows a decreasing behaviour. Rather than the expected high-Re trend, the most striking feature of Fig. 4 (right) is the tendency of both $\langle \Delta z_g \rangle$ and $\langle \Delta z_r \rangle$ to grow large at low Re, up to much larger values than the width of a streak. This confirms the observation that a large set of streaks can be either gained or lost brutally near the interface, consistently with an increase of the spanwise correlation length at low Re.

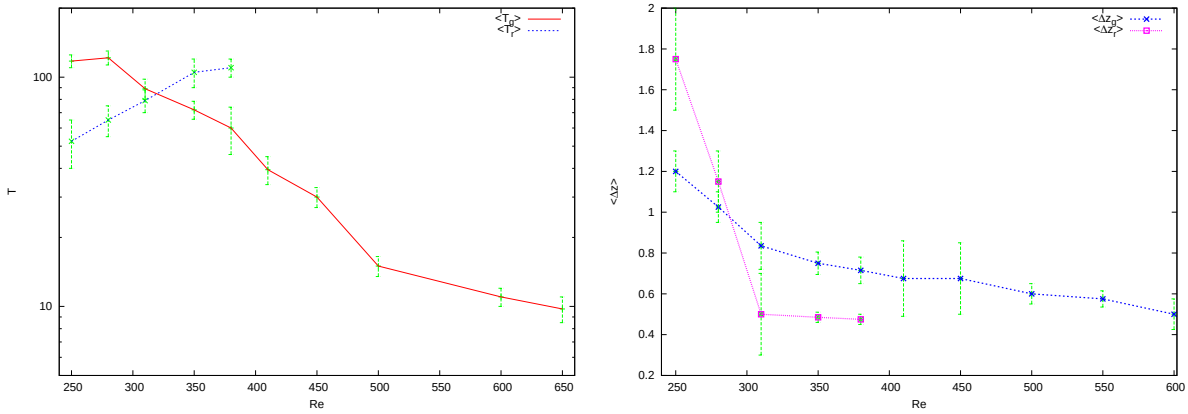

FIG. **4.** Mean waiting times (left) and mean jump length (right) vs. Re.

2 Depinning transition

The results of the previous section point out that the assumption for Gaussianity breaks down for the lowest values of Re. From $Re \sim 280$ down to $Re = 217 \pm 1$, some unexpected non-trivial (not necessary "turbulent") dynamics is observed, characterised by phases of regular growth over a time much longer than predicted by low-Re extrapolation of the previous distributions (see Figure 5). These long growth phases are very reminiscent of the depinning transition predicted in the vicinity of a homoclinic snaking

region in extended one-dimensional systems parametrised by one governing parameter r (see Figure 14 in Ref. [1]). Homoclinic snaking is observed in ordinary differential equations where a non-trivial ("patterned") steady state with a spatially periodic structure bifurcates subcritically from a trivial homogeneous ("laminar") solution. The non-trivial branch then bifurcates into two branches which can be traced down the governing parameter and begin to intertwingle inside a narrow range $[r_1 : r_2]$, giving rise to a multiplicity of steady localised states pinned to the non-localised patterned state. Analysis in the case of the Swift-Hohenberg equation has shown that for $0 < \delta = r - r_2 << 1$, depinning of the fronts occurs, i.e. the fronts are no longer stationary yet drift so that the patterned state invades the whole domain, with a velocity scaling as $O(\delta^{\frac{1}{2}})$) (see Figure 14 in Ref. [1]). Recently, Schneider et al. have considered the case of pCf with periodic boundary conditions in x and z with extension in the z direction, taking $(L_x, L_z) = (4\pi, 16\pi)$ [6]. This is qualitatively very similar to the quasi-1D geometry considered here. They have identified a snaking region in a interval $[Re_{s1} : Re_{s2}] \approx [170 : 175]$ containing a series of z-localised solutions, either steady of travelling slowly in the x-direction. More recently, these authors have investigated the L_z-dependence of the snaking interval, showing that Re_{s2} rapidly increases with decreasing L_z, suggesting the range $\approx 201 - 213$ for $L_z = 10.417 \approx 3.3\pi$ [4].

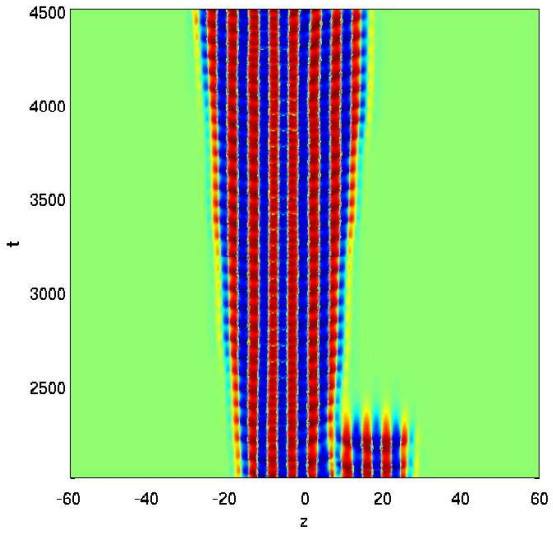

FIG. **5.** Space-time (z, t) diagram for the quantity $Y(z, t)$; Re=220

In order to verify that the long phases of growth are related to the depinning transition, a set of simulations has been analysed for several values of Re between 190 and 280, all starting from the same turbulent state obtained in a previous run at Re =250. Since we are interested here in long growth phases rather than on retreat/progress events on a short time-scale, we have deliberately selected only growth events with a constant velocity on a time scale $\Delta T > 1000$. An interpolation is then performed directly from space-time- diagrams such as the one in Fig. 5, yielding the front velocity $c = \frac{\Delta z}{\Delta T}$. We have checked that c scales like $O(\sqrt{Re - Re_{s2}})$, with Re_{s2} given by $\approx 217 \pm 1$ (see Figure 6). The match with available data is thus very satisfying, especially given the discrepancy in the values of L_x considered.

3 Conclusions

We have investigated the dynamics of a laminar-turbulent interface in plane Couette flow, in the special case where the interface is parallel to the mean flow direction. The motion appears as a stochastic process above $Re \geq 280$, with an average speed increasing from negative values at low Re to positive values

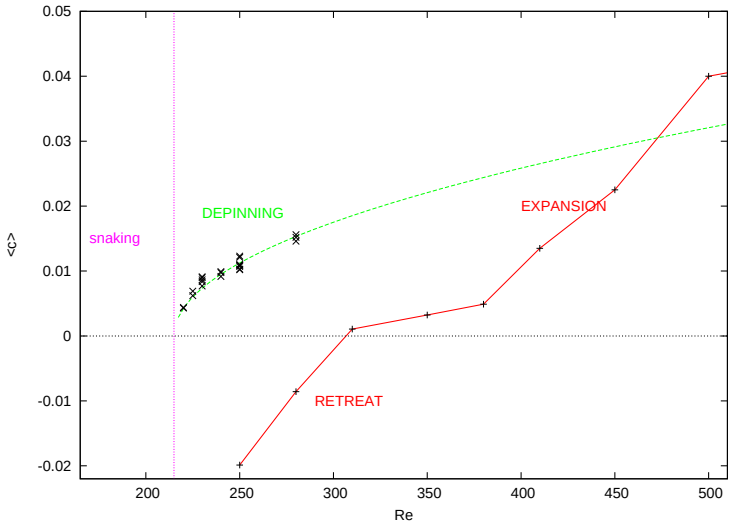

FIG. **6.** Bifurcation diagram showing the competition between the deterministic depinning branch and the stochastic branch

at higher Re. Interestingly, the front velocity reaches a plateau for $Re \approx [320 : 410]$, which corresponds to the range of Re at which robust laminar/turbulent patterns are observed in experiments [3,7]. It is not excluded that the extra advection by the large-scale flow induced by turbulent fluctuations could stabilise the motion of the fronts and thus explain the robustness of the patterns. For lower values of Re, stochasticity is observed to compete with a deterministic dynamics, which we interprete as a depinning transition from the homoclinic snaking regime already identified using an other approach (as in Figure 6). Whether stochastic and deterministic branches bifurcate one from another or whether these are two disconnected phenomena remains to be investigated.

Références

1. J. BURKE & E. KNOBLOCH, Localized states in the generalized Swift-Hohenberg equation, *Physical Review E*, **73**, 056211 (2006).
2. O. DAUCHOT & F. DAVIAUD, Finite amplitude perturbation and spots growth mechanism in plane Couette flow, *Physics of Fluids*, **7**, 335-343 (1995).
3. Y. DUGUET, P. SCHLATTER & D. S. HENNINGSON, Formation of turbulent patterns near the onset of transition in plane Couette flow, *Journal of Fluid Mechanics*, **650**, 119-129 (2010).
4. J. F. GIBSON, *private communication* (2011).
5. E. W. MONTROLL & G. H. WEISS, Random walks on lattices, *Journal of Mathematical Physics*, **6**, 167 (1965).
6. T. M. SCHNEIDER, J. F. GIBSON & J. BURKE, Snakes and ladders : localized solutions of plane Couette flow, *Physical Review Letters*, **104**, 104501 (2010).
7. L. S. TUCKERMAN & D. BARKLEY, Turbulent-laminar patterns in plane Couette flow, *IUTAM Symposium on Laminar-Turbulent Transition and Finite Amplitude Solutions*, Eds. T. Mullin & R. Kerswell, pp. 107–127, Springer, Dordrecht (2005).